



Staphylococcus aureus HemX Modulates Glutamyl-tRNA Reductase Abundance To Regulate Heme Biosynthesis

Jacob E. Choby,^{a,b,c} Caroline M. Grunenwald,^{a,b} Arianna I. Celis,^d Svetlana Y. Gerdes,^e Jennifer L. DuBois,^d Eric P. Skaar^{a,b}

^aDepartment of Pathology, Microbiology, & Immunology, Vanderbilt University Medical Center, Nashville, Tennessee, USA

^bVanderbilt Institute for Infection, Immunology, and Inflammation, Vanderbilt University Medical Center, Nashville, Tennessee, USA

^cGraduate Program in Microbiology & Immunology, Vanderbilt University, Nashville, Tennessee, USA

^dDepartment of Chemistry and Biochemistry, Montana State University, Bozeman, Montana, USA

^eFellowship for Interpretation of Genomes, Burr Ridge, Illinois, USA

ABSTRACT *Staphylococcus aureus* is responsible for a significant amount of devastating disease. Its ability to colonize the host and cause infection is supported by a variety of proteins that are dependent on the cofactor heme. Heme is a porphyrin used broadly across kingdoms and is synthesized *de novo* from common cellular precursors and iron. While heme is critical to bacterial physiology, it is also toxic in high concentrations, requiring that organisms encode regulatory processes to control heme homeostasis. In this work, we describe a posttranscriptional regulatory strategy in *S. aureus* heme biosynthesis. The first committed enzyme in the *S. aureus* heme biosynthetic pathway, glutamyl-tRNA reductase (GtrR), is regulated by heme abundance and the integral membrane protein HemX. GtrR abundance increases dramatically in response to heme deficiency, suggesting a mechanism by which *S. aureus* responds to the need to increase heme synthesis. Additionally, HemX is required to maintain low levels of GtrR in heme-proficient cells, and inactivation of *hemX* leads to increased heme synthesis. Excess heme synthesis in a Δ *hemX* mutant activates the staphylococcal heme stress response, suggesting that regulation of heme synthesis is critical to reduce self-imposed heme toxicity. Analysis of diverse organisms indicates that HemX is widely conserved among heme-synthesizing bacteria, suggesting that HemX is a common factor involved in the regulation of GtrR abundance. Together, this work demonstrates that *S. aureus* regulates heme synthesis by modulating GtrR abundance in response to heme deficiency and through the activity of the broadly conserved HemX.

IMPORTANCE *Staphylococcus aureus* is a leading cause of skin and soft tissue infections, endocarditis, bacteremia, and osteomyelitis, making it a critical health care concern. Development of new antimicrobials against *S. aureus* requires knowledge of the physiology that supports this organism's pathogenesis. One component of staphylococcal physiology that contributes to growth and virulence is heme. Heme is a widely utilized cofactor that enables diverse chemical reactions across many enzyme families. *S. aureus* relies on many critical heme-dependent proteins and is sensitive to excess heme toxicity, suggesting *S. aureus* must maintain proper intracellular heme homeostasis. Because *S. aureus* provides heme for heme-dependent enzymes via synthesis from common precursors, we hypothesized that regulation of heme synthesis is one mechanism to maintain heme homeostasis. In this study, we identify that *S. aureus* posttranscriptionally regulates heme synthesis by restraining abundance of the first heme biosynthetic enzyme, GtrR, via heme and the broadly conserved membrane protein HemX.

KEYWORDS *Staphylococcus aureus*, heme, tetrapyrroles

Received 22 December 2017 Accepted 8

January 2018 Published 6 February 2018

Citation Choby JE, Grunenwald CM, Celis AI, Gerdes SY, DuBois JL, Skaar EP. 2018.

Staphylococcus aureus HemX modulates glutamyl-tRNA reductase abundance to regulate heme biosynthesis. mBio 9:e02287-17. <https://doi.org/10.1128/mBio.02287-17>.

Editor Kimberly A. Kline, Nanyang Technological University

Copyright © 2018 Choby et al. This is an open-access article distributed under the terms of the [Creative Commons Attribution 4.0 International license](https://creativecommons.org/licenses/by/4.0/).

Address correspondence to Eric P. Skaar, eric.skaar@vanderbilt.edu.

This article is a direct contribution from a Fellow of the American Academy of Microbiology. Solicited external reviewers: Anthony Richardson, University of Pittsburgh; David Heinrichs, University of Western Ontario.

The tetrapyrrole cofactor heme is critical to the physiology of organisms from humans to bacteria. Heme is composed of a porphyrin ring complexed to iron at its center, making it an excellent redox-active moiety for a variety of enzymes. Across kingdoms, heme is used to shuttle electrons in the respiratory chain and is also required for the function of many critical proteins, including nitric oxide synthase, catalase, and hemoglobin. To satisfy the cellular need for heme, most heme-dependent organisms synthesize heme *de novo* from simple and abundant precursors.

The versatility of heme as a cofactor is based on its reactivity, which also results in its toxicity at high concentrations. Excess heme can cause damage to cellular macromolecules, and the redox cycling of heme-iron produces reactive oxygen species via Fenton chemistry (1). Bacteria encode a variety of mechanisms to resist heme toxicity (1), but the most important of these strategies may be the prevention of self-imposed toxicity by regulating endogenous heme synthesis. A variety of transcriptional and posttranscriptional strategies have evolved to regulate heme synthesis centered around providing sufficient heme to occupy hemoproteins while preventing excess heme synthesis to limit unnecessary consumption of substrates and preclude toxicity.

In this study, we sought to uncover regulatory pathways controlling heme synthesis in the human pathogen *Staphylococcus aureus*. *S. aureus* is a Gram-positive bacterium that causes a variety of devastating diseases, including skin and soft tissue infections, osteomyelitis, endocarditis, and bacteremia (2). *S. aureus*, as a facultative anaerobe, generates energy through aerobic respiration, anaerobic respiration, or fermentation. The final step in aerobic respiration is reduction of oxygen to water, which *S. aureus* performs with either of the heme-dependent QoxABCD or CydAB terminal oxidases (3, 4). Although a great deal is known about heme synthesis, heme utilization, and heme toxicity in *S. aureus*, no heme synthesis regulatory pathway has been identified in this organism. *S. aureus* encodes the newly appreciated coproporphyrin-dependent heme synthesis pathway to populate its hemoproteins (5, 6). These include the terminal oxidases, catalase, and bacterial nitric oxide synthase, all of which contribute to growth, protection from host defenses, and pathogenesis (3, 7–9). Under conditions of excess exogenous heme, the heme stress response in *S. aureus* is activated by the heme-sensing two-component system HssRS, which regulates the transcription of a putative efflux pump, HrtAB. This system is critical for growth and survival in toxic concentrations of heme and modulates pathogenesis in a murine model of disease (10). Sensing or regulatory pathways that connect heme synthesis with heme availability, hemoprotein abundance, or HssRS activation have not been identified.

S. aureus synthesizes δ -aminolevulinic acid (ALA), the first dedicated and universal precursor for protoheme synthesis, via the conversion of glutamyl-tRNA to glutamate-1-semialdehyde by glutamyl-tRNA reductase (GtrR) and subsequent production of ALA by glutamate-1-semialdehyde 2,1-aminomutase (11–13). Uroporphyrinogen is the precursor to heme, siroheme, and other tetrapyrroles, and the stepwise transformation of ALA to uroporphyrinogen comprises the core of the synthesis pathway. The pathway from uroporphyrinogen to heme was historically considered to be universally conserved for all organisms. However, the field's understanding of bacterial heme synthesis has undergone a revolution as recent studies uncovered diversity in bacterial strategies to convert uroporphyrinogen to heme (reviewed in reference 14). Gram-positive bacteria proceed through a coproporphyrin-dependent branch (5, 6, 15) that is unique from the classic protoporphyrin-dependent branch in humans and many Gram-negative model organisms.

In this work, we identify GtrR abundance as a critical regulator of *S. aureus* heme synthesis. GtrR is posttranscriptionally maintained at low abundance in heme-proficient cells by the membrane protein HemX, but levels increase when *S. aureus* is deprived of heme. Without HemX regulation, GtrR abundance increases, which results in the concomitant increase in flux through the heme synthesis pathway and accumulation of heme. This excess heme synthesis activates HssRS and disrupts iron homeostasis. Together, this report reveals that *S. aureus* regulates heme synthesis by modulating GtrR abundance via intracellular heme levels and the widely conserved HemX.

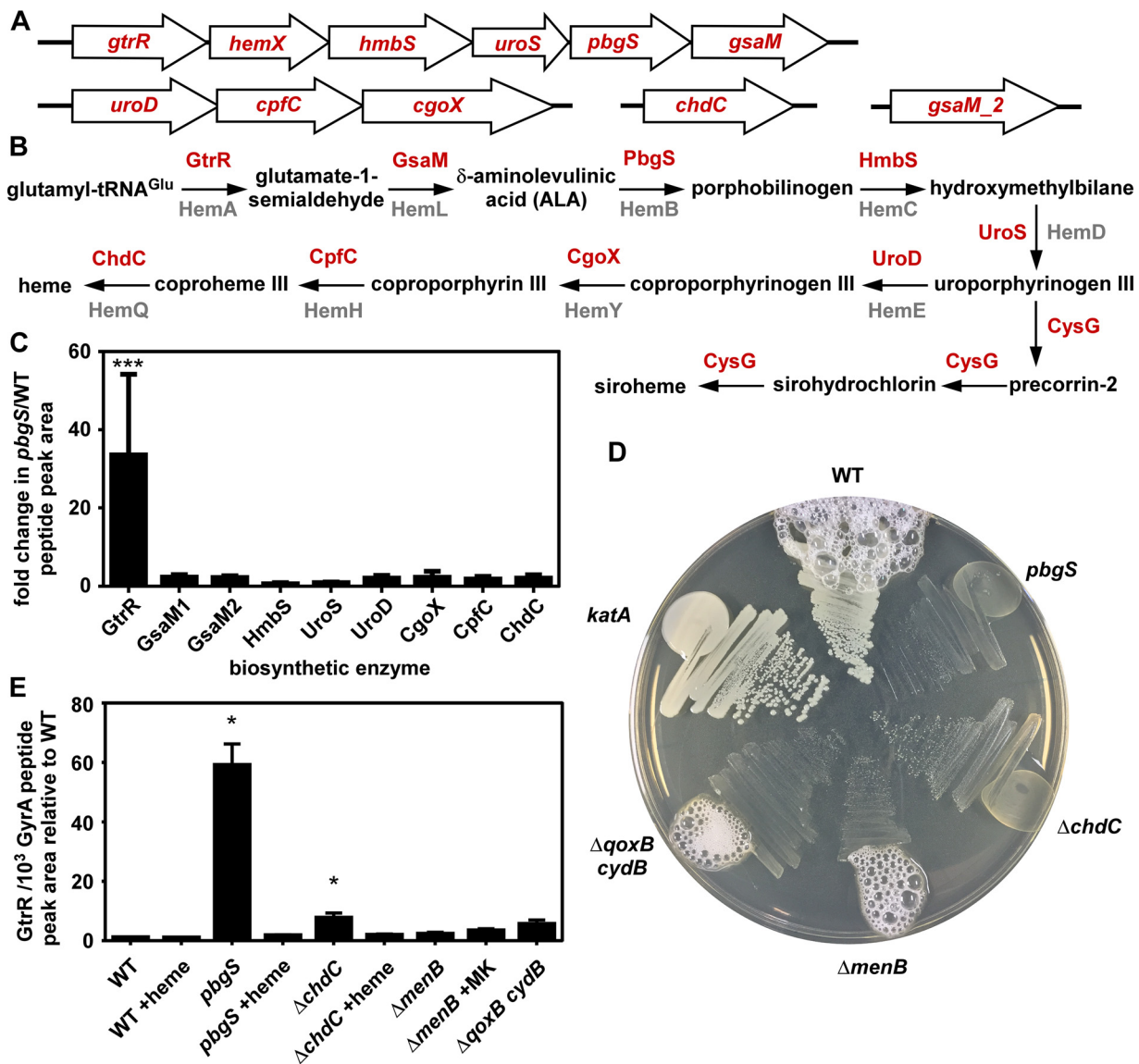


FIG 1 Heme deficiency increases GtrR abundance. (A) The genes encoding heme biosynthesis enzymes are located at four chromosomal loci. (B) An overview of the *S. aureus* heme and siroheme biosynthetic pathway. In red are the updated enzyme names set forth by Dailey and colleagues (14), which correspond to the previously used gene locus names in gray. (C) The abundance of each biosynthetic enzyme was measured by LC-MRM-MS/MS and quantified by integrated chromatogram peak areas. Graphed is the ratio of each enzyme's abundance in a strain lacking *pbgS* relative to WT *S. aureus*; the data are the average from a single experiment performed in biological triplicate with standard deviation shown. Statistical significance was determined using a one-way analysis of variance (ANOVA) with Dunnett's correction for multiple comparisons, using a reference value of 1.0. ***, $P < 0.001$. (D) The *S. aureus* strains listed were streaked onto rich agar medium plates, and after growth, hydrogen peroxide was added at the perimeter of each streak. (E) The abundance of GtrR was measured by LC-MRM-MS/MS in *S. aureus* strains treated with vehicle, heme, or menaquinone (MK). The data are the average from a single experiment performed in biological triplicate with standard deviation shown. Statistical significance was determined using a one-way ANOVA with Dunnett's correction for multiple comparisons, comparing GtrR abundance for each condition relative to the WT. *, $P < 0.05$.

RESULTS

GtrR abundance increases specifically in response to heme deficiency. To identify key steps in the regulation of heme synthesis (Fig. 1A and B), we measured the abundance of each biosynthetic enzyme by liquid chromatography-multiple reaction monitoring-tandem mass spectrometry (LC-MRM-MS/MS). This technique allows for quantification with high resolution of even very-low-abundance cellular proteins (16). We hypothesized that comparing the *S. aureus* wild type (WT) to a strain incapable of synthesizing heme (*pbgS* mutant) (Fig. 1A and B) would allow the identification of specific steps in heme synthesis that respond to cellular heme content, directly or

indirectly. Abundance of GtrR is approximately 30-fold higher in the *pbgS* mutant relative to the WT, while the abundances of all other biosynthetic enzymes are nearly unchanged (Fig. 1C). In WT cells, GtrR abundance is low relative to other heme synthesis enzymes (see Fig. S1 in the supplemental material). The *pbgS* mutant is a heme auxotroph and therefore adopts the respiration-deficient small-colony variant (SCV) phenotype. SCVs arise as the result of inactivation of respiration via inactivation of heme synthesis, the terminal oxidases, or the electron carrier menaquinone, and SCVs have a dramatically different physiology than respiration-proficient cells (17). Therefore, we sought to determine whether the increase in GtrR abundance in the *pbgS* mutant was the result of heme deficiency or a general defect in respiration. To confirm that the menaquinone auxotroph SCV $\Delta menB$ strain and the $\Delta qoxB$ *cydB* strain lacking both terminal cytochrome oxidases synthesize heme despite being unable to respire, each strain was streaked onto agar and assessed for catalase activity (Fig. 1D). Activity of the heme-dependent catalase KatA leads to the production of oxygen bubbles when hydrogen peroxide is added. The $\Delta menB$ and $\Delta qoxB$ *cydB* mutants produce bubbles, demonstrating that these SCVs synthesize heme and are not heme auxotrophs. We measured GtrR abundance in a variety of SCV strains by LC-MRM-MS/MS. GtrR abundance increases relative to the WT only in *pbgS* and $\Delta chdC$ strains (Fig. 1B and E), which are heme auxotroph SCVs (Fig. 1D). When chemically complemented with heme, GtrR abundance returned to WT levels for both strains. GtrR levels do not increase in the $\Delta menB$ or $\Delta qoxB$ *cydB* strain. Together these data demonstrate that the abundance of GtrR is low in heme-proficient cells but increases specifically in response to heme deficiency.

HemX controls GtrR abundance in heme-proficient cells to regulate heme synthesis. Among both Gram-negative and Gram-positive bacteria, regulation of GtrR abundance is a common feature of heme synthesis regulation pathways (18–20). In the model organism *Bacillus subtilis*, which is also a member of the *Firmicutes* phylum, GtrR abundance is impacted by the membrane protein HemX through an unknown mechanism (18, 21). While *S. aureus* is in the same *Bacillales* order as *B. subtilis*, *S. aureus* heme homeostasis is distinct because of its access to host heme and its resistance to heme toxicity mediated by HssRS. Both *B. subtilis* and *S. aureus* carry an operon comprised of *gtrR-hemX-hmbS-uroS-pgbS-gsaM* (formerly *hemAXCBDL*) (22, 23). We therefore hypothesized that in *S. aureus*, HemX also impacts GtrR abundance in heme-proficient cells. We created an in-frame unmarked deletion of *hemX* and integrated either pJC1111 P_{igt} or $P_{igt}hemX$ at a neutral site in the chromosome (24). GtrR abundance was measured by LC-MRM-MS/MS and is increased in the $\Delta hemX::P_{igt}$ strain relative to WT:: P_{igt} (Fig. 2A). The phenotype can be complemented when *hemX* is provided in *cis*, showing that it is the result of deletion of *hemX* and not other effects of disrupting the operon. These data are consistent with the hypothesis that HemX regulates GtrR abundance in heme-proficient cells (18, 21).

We next sought to determine whether the increase in GtrR at the protein level in both the *pbgS* and $\Delta hemX$ strains is the result of an increase in mRNA transcript abundance of *gtrR*. Therefore, the *pbgS* and $\Delta hemX$ strains were grown to the mid-exponential phase, and RNA was isolated, converted to cDNA, and quantified by quantitative PCR (qPCR) (Fig. 2B). The steady-state mRNA abundance of *gtrR* transcript is unchanged in the $\Delta hemX$ or *pbgS* strain relative to the WT, suggesting that the increase in GtrR abundance in these strains is not the result of a transcriptional change. Additionally, the increase in GtrR levels in the *pbgS* strain is not affected by the insertion of *ermB* to interrupt the *pbgS* gene, which is upstream of *gsaM* in the operon; there is no change in the transcript abundance of *gsaM* in the *pbgS* strain relative to the WT (see Fig. S2 in the supplemental material).

We hypothesized that the increase in GtrR observed in the $\Delta hemX$ strain would increase the amount of heme synthesized by increasing abundance of the heme precursors downstream of GtrR. As glutamate-1-semialdehyde is unstable and can convert to δ -aminolevulinic acid (ALA) in the absence of enzyme (25), we measured ALA abundance via a colorimetric method. ALA abundance increases approximately 50% in

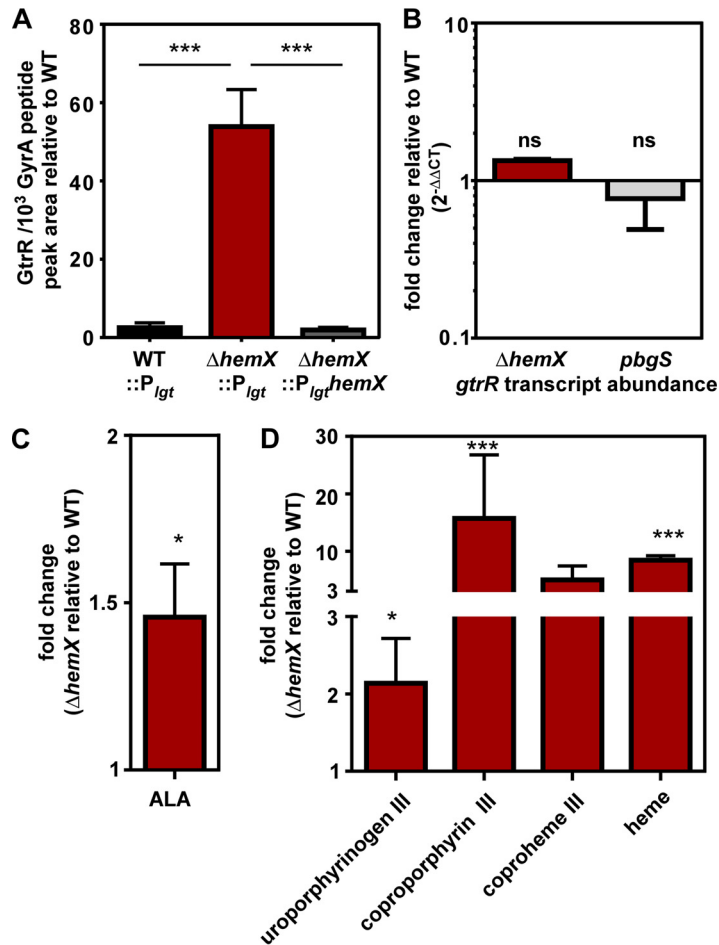


FIG 2 HemX regulates heme synthesis by maintaining low levels of GtrR in heme-proficient cells. (A) The abundance of GtrR was measured by LC-MRM-MS/MS in multiple *S. aureus* strains. The data are the average from a single experiment performed in biological triplicate with standard deviation shown. Statistical significance was determined using a one-way ANOVA with Dunnett's correction for multiple comparisons, comparing GtrR abundance for each strain relative to the $\Delta hemX::P_{lgt}$ strain. ***, $P < 0.001$. (B) Steady-state transcript abundance of *gtrR* mRNA isolated from mid-exponential growth of *S. aureus* strains was measured by qRT-PCR and is graphed as fold change relative to the WT. Data are combined from two independent experiments in biological triplicate with standard deviation shown. "ns" indicates no significance by one-way ANOVA with Dunnett's correction for multiple comparisons, comparing fold change of the *pbgS* and $\Delta hemX$ strains to the WT. (C) δ -Aminolevulinic acid (ALA) abundance was measured in *S. aureus* strains by a spectrophotometric quantification. Graphed is the fold change of ALA in the $\Delta hemX$ mutant relative to the WT, with data combined from two independent experiments with three biological replicates with standard error of the mean shown. (D) Uroporphyrinogen III (detected as uroporphyrin III), coproporphyrin III, coproheme III, and heme were quantified by LC-qTOF-MS. Graphed is the fold change of metabolite abundance in the $\Delta hemX$ mutant relative to the WT, from a single experiment performed in biological triplicate with standard error of the mean shown. For panels C and D, statistical significance was determined with Student's *t* test comparing the $\Delta hemX$ mutant to the WT before data transformation to fold change. *, $P < 0.05$; ***, $P < 0.0001$.

the $\Delta hemX$ strain relative to the WT (Fig. 2C). We subsequently sought to determine the impact of increased ALA availability on downstream heme intermediates and heme abundance. Total cellular porphyrins were extracted from the WT and $\Delta hemX$ strains and analyzed by quantitative exact-mass liquid chromatography-quadrupole time of flight mass spectrometry (LC-qTOF-MS); total extracted ion chromatograms for porphyrins that were observed above the limits of detection are shown in Fig. S3 in the supplemental material, where a dramatic change in porphyrin levels is visible. Based on standard curves for individual porphyrins (including porphobilinogen, uroporphyrins I and III, coproporphyrins I and III, coproheme III, protoporphyrin IX, and heme b) and enumeration of colony-forming units, absolute quantifications were obtained and

referenced per cell for each porphyrin molecule; data are presented in Fig. 2D in terms of fold change relative to the WT. As shown in Fig. 2D; the $\Delta hemX$ strain exhibits increased abundance of uroporphyrin III, coproporphyrin III, coproheme III, and heme *b* relative to the WT. Notably, because samples were prepared aerobically, the metabolite uroporphyrinogen III was detected as uroporphyrin III, in which its methylene bridge carbons have spontaneously oxidized in air; likewise, any coproporphyrinogen III that might have been present would be detected as the oxidation product, coproporphyrin III, which is also the product of the enzyme CgoX (Fig. 1). Hydroxymethylbilane spontaneously cyclizes to uroporphyrinogen I, which is decarboxylated by UroD to coproporphyrinogen I. The absence of uroporphyrin or coproporphyrin I isomers indicates that hydroxymethylbilane did not accrue in the $\Delta hemX$ mutant. We hypothesize that, in the presence of excess GtrR, the initial step of the pathway may no longer be rate limiting. This may allow other subsequent steps in the pathway to become partly rate limiting, leading to the observed pattern of metabolite accumulation. Finally, the increase in heme abundance in the $\Delta hemX$ strain observed by LC-qTOF-MS is complemented when *hemX* is provided in *cis* from a neutral site in the chromosome, as measured by the pyridine hemochromagen method (see Fig. S4A in the supplemental material). Together, these data demonstrate that inactivation of *hemX* results in increased GtrR abundance, which increases abundances of both early- and late-pathway biosynthetic precursors and cellular heme. Therefore, dysregulation of GtrR alone is sufficient to disrupt heme homeostasis.

Excess endogenous heme synthesis in the $\Delta hemX$ mutant activates the heme stress response. The unregulated GtrR abundance in the $\Delta hemX$ mutant results in greater cellular heme levels (Fig. 2D), which we hypothesized would activate the heme sensor system HssRS in the absence of exogenous heme, leading to transcriptional induction of the *hrtAB* efflux pump. The WT and $\Delta hemX$ mutant strains were transformed with plasmids containing the luminescence-producing operon *luxABCDE* cloned from *Photobacterium luminescens* without a promoter (pXen-1) or controlled by the HssRS-regulated promoter P_{hrt} . P_{hrt} promoter activity, visualized by luminescent imaging, shows that HssRS is activated in the $\Delta hemX$ strain in the absence of exogenous heme, whereas HssRS is not activated in the WT (Fig. 3A). The $P_{hrt}lux$ activity in WT becomes apparent when 20 μM exogenous heme is added to the agar medium, and luminescence depends on the heme-responsive P_{hrt} . To more quantitatively measure P_{hrt} activity as a readout of HssRS activation by endogenous heme, we transformed WT, $\Delta hemX$, and $\Delta hssRS$ strains with the pOS1 $P_{hrt}xylE$ plasmid. These strains report P_{hrt} activity with the production of the XylE catechol oxidase enzyme, which can be quantified spectrophotometrically from cell lysate. Data in Fig. 3B demonstrate that in the absence of exogenous heme, P_{hrt} is induced in the $\Delta hemX$ strain. P_{hrt} activity does increase in the WT and $\Delta hemX$ strains in a dose-dependent manner as exogenous heme is added, but P_{hrt} activity remains higher in the $\Delta hemX$ mutant than the WT at all tested heme concentrations. Additionally, XylE activity in this system is dependent on the HssRS two-component system. Taken together, these data suggest that excess endogenous heme synthesized in the $\Delta hemX$ strain is sufficient to activate the HssRS two-component system.

We next hypothesized that the intermediate levels of HssRS activation in the $\Delta hemX$ mutant, in the absence of exogenous heme (Fig. 3A and B), would be sufficient to preadapt the $\Delta hemX$ mutant to heme toxicity. As the HssRS-HrtAB heme stress response provides resistance to heme toxicity, pretreatment with subtoxic concentrations of heme adapts *S. aureus* to subsequent growth in toxic concentrations of heme by activating HssRS and increasing the abundance of HrtAB (10). The WT grown in 10 μM heme without preadaptation has a severe growth defect evident by a 6-h lag time (Fig. 3C). When preadapted in 2 μM heme, the WT demonstrates a reduced lag time and greater overall growth, albeit at a lower rate and yield than when grown without heme. In contrast, the $\Delta hemX$ mutant grown in 10 μM heme with or without preadaptation exhibits increased growth compared to the WT. The enhanced growth of the $\Delta hemX$ mutant in 10 μM heme is dependent on the HrtAB efflux system, as the $\Delta hemX$

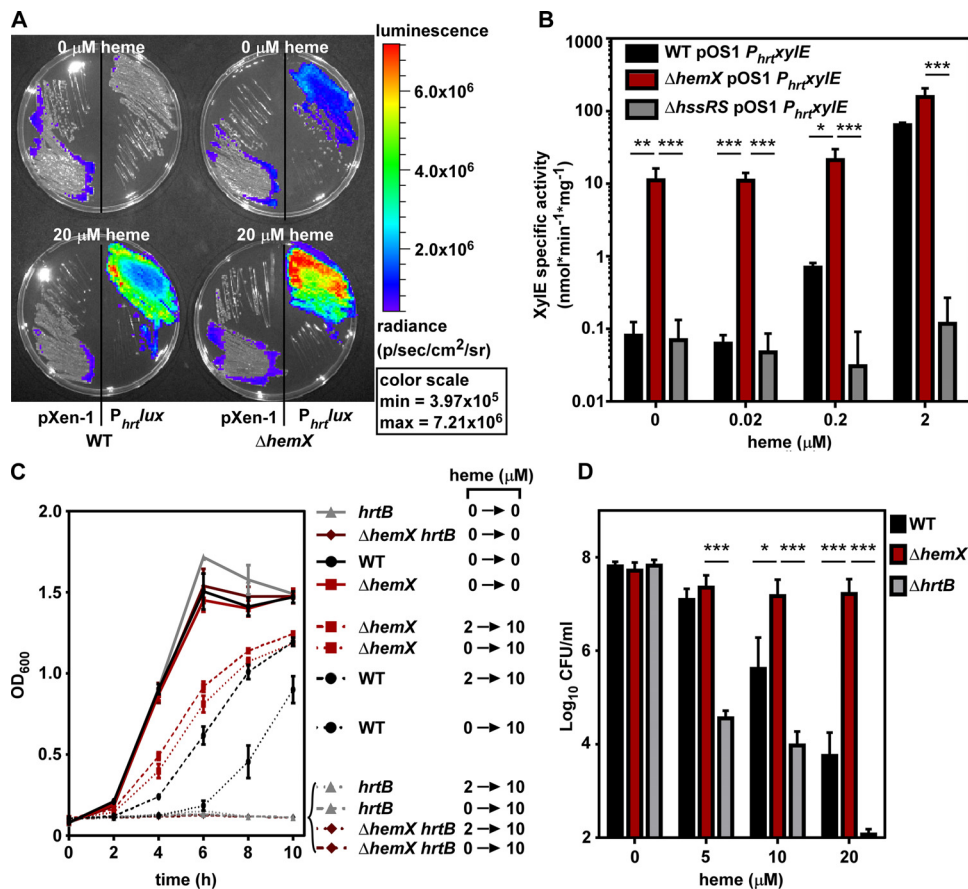


FIG 3 Excess heme synthesis in the $\Delta hemX$ mutant activates the heme stress response. (A) Bioluminescence was imaged on agar medium plates containing vehicle or heme onto which strains were streaked. All four plates were imaged simultaneously, and luminescence was converted to a heat map with the scale shown on the right. (B) XylE catechol oxidase activity was measured in *S. aureus* strains after growth in vehicle or increasing concentrations of heme. The data are the average from three independent experiments each in biological triplicate with standard deviation shown. Statistical significance was determined using a two-way ANOVA with Tukey's correction for multiple comparisons, comparing log-transformed data for the $\Delta hemX$ pOS1 $P_{hrt}xylE$ strain at each heme concentration to that of each other strain. *, $P < 0.01$; **, $P < 0.001$; ***, $P < 0.0001$. (C) Growth as measured by OD₆₀₀ was monitored over time for *S. aureus* strains in medium containing either vehicle or 10 μM heme. Prior to the measured growth, the strains were pregrown to the stationary phase in medium containing vehicle or 2 μM heme. The data are the average of the means from at least three independent experiments each in biological triplicate with standard error of the mean shown. (D) Viable bacteria from *S. aureus* strains were enumerated after incubation for 2 h in medium containing vehicle or increasing amounts of heme. The data are the average of the means from three independent experiments each in biological triplicate with standard error of the mean shown. The y axis is set to the limit of detection. Statistical significance was determined using a two-way ANOVA with Tukey's correction for multiple comparisons, comparing log-transformed data for the WT and $\Delta hrtB$ strains to the $\Delta hemX$ mutant at each heme concentration. *, $P < 0.01$; ***, $P < 0.0001$.

hrtB strain does not grow in 10 μM heme (Fig. 3C). Additionally, preadaptation of the $\Delta hemX$ strain in this assay can be complemented by providing *hemX* in the chromosome (Fig. S4B). Similarly, the $\Delta gtrR$ -*hemX* pOS1 $P_{gtr}gtrR$ strain is resistant to heme toxicity, but becomes sensitive again when *hemX* is introduced on the plasmid (Fig. S4C). This is further evidence that HemX control of GtrR is not transcriptional, as HemX exerts its effect independent of the native *gtrR* promoter and ribosome binding site in this assay. Further, the $\Delta hemX$ mutant is resistant to the bactericidal effects of acute heme toxicity, compared to a 4-log reduction in viable WT cells after 2 h in the presence of 20 μM heme (Fig. 3D). In sum, these data demonstrate that increased cellular heme in the $\Delta hemX$ mutant is sufficient to activate HssRS and cause expression of HrtAB, which leads to resistance to heme toxicity.

Excess heme synthesis disrupts iron homeostasis. Considering that every molecule of heme contains an atom of iron, we hypothesized that unregulated heme

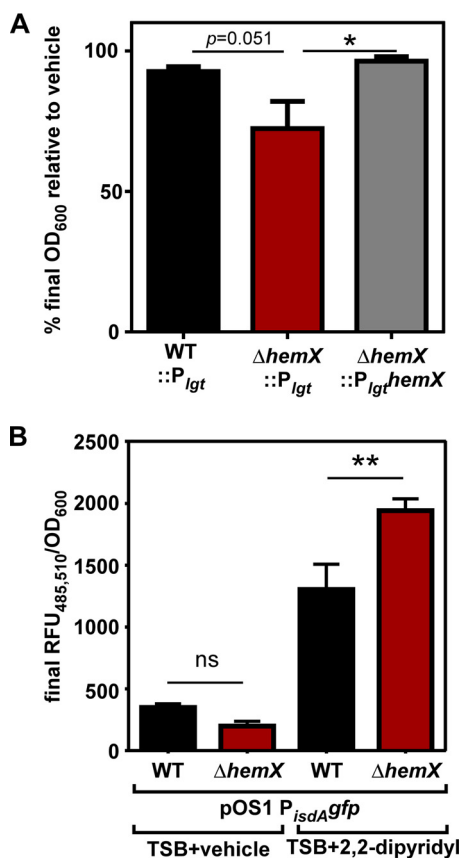


FIG 4 Unregulated heme synthesis alters iron homeostasis. (A) Growth was measured in minimal medium containing vehicle or 1 μ M iron chelator EDDHA. Graphed is the final growth as measured by the OD₆₀₀ for each *S. aureus* strain in medium containing EDDHA relative to vehicle. The data are the average of the means from five independent experiments each in at least biological triplicate with standard error of the mean shown. Statistical significance was determined using a one-way ANOVA with Dunnett's correction for multiple comparisons, comparing the Δ hemX::P_{lgt} strain to each other strain. *, $P < 0.05$. (B) The activity of the iron limitation-responsive promoter P_{isdA} was measured by recording fluorescence intensity over time in rich medium containing vehicle or the iron chelator 2,2-dipyridyl. The data are the average of the means from three independent experiments each in biological triplicate with standard error of the mean shown. Statistical significance was determined using a one-way ANOVA with Sidak's correction for multiple comparisons, comparing data for the WT and Δ hemX mutant under each condition. **, $P < 0.01$; ns, not significant.

synthesis in the Δ hemX mutant would consume high levels of iron and alter iron homeostasis. To test this hypothesis, growth in minimal medium containing the iron chelator EDDHA [ethylenediamine-*N,N'*-bis(2-hydroxyphenylacetic acid)] was compared to growth in minimal medium alone. As shown in Fig. 4A, the Δ hemX::P_{lgt} strain demonstrates reduced total yield after growth for 24 h relative to WT::P_{lgt} and the complemented Δ hemX::P_{lgt}hemX strain. To corroborate this finding, we assessed promoter activity using a P_{isdA}gfp reporter plasmid. P_{isdA} is controlled by the ferric uptake regulator (Fur) and is derepressed under iron-depleted conditions (26). Data in Fig. 4B show that after growth in rich medium with an alternative iron chelator, 2,2-dipyridyl, the Δ hemX pOS1 P_{isdA}gfp strain has enhanced P_{isdA} activity relative to WT pOS1 P_{isdA}gfp. These data suggest excess heme synthesis depletes the cell of available iron.

Inactivation of HemX reduces GtrR abundance in heme deficiency. Based on the observations that HemX and cellular heme both impact GtrR abundance, we hypothesized that measuring GtrR abundance in a strain lacking hemX and unable to synthesize heme would uncover the nature of the relationship between HemX, heme, and GtrR. Surprisingly, GtrR abundance in the Δ hemX pbgS strain is unchanged from that in the Δ hemX strain and lower than that in the pbgS strain (Fig. 5A), and this effect is not

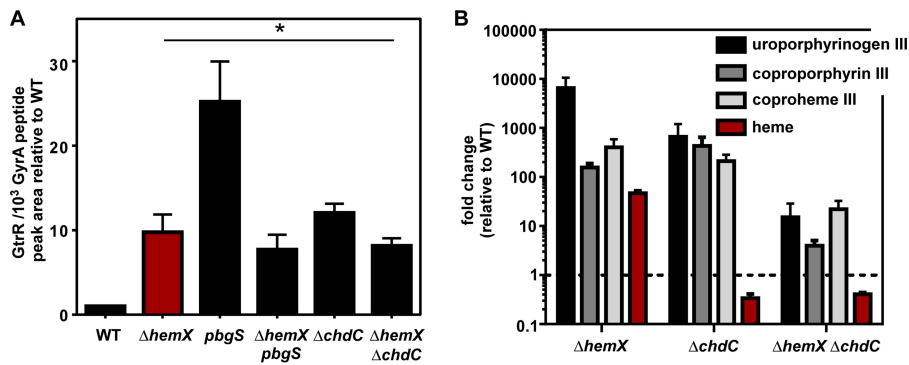


FIG 5 Inactivation of HemX reduces GtrR abundance in heme-deficient strains. (A) The abundance of GtrR was measured by LC-MRM-MS/MS in multiple *S. aureus* strains. The data are the average from a single experiment performed in biological triplicate with standard deviation shown. Statistical significance was determined using a one-way ANOVA with Dunnett's correction for multiple comparisons, comparing GtrR abundance for each strain relative to WT. *, $P < 0.05$. (B) Uroporphyrinogen III (detected as uroporphyrin III), coproporphyrin III, coproheme III, and heme were quantified by LC-qTOF-MS. Graphed is the fold change of metabolite abundance in each mutant relative to the WT from a single experiment performed in biological triplicate with standard error of the mean shown.

the result of a change in *gtrR* transcription in the $\Delta hemX pbgS$ strain relative to the *pbgS* strain (see Fig. S5 in the supplemental material). Similarly, the $\Delta hemX \Delta chdC$ mutant has lower levels of GtrR than the $\Delta chdC$ mutant (Fig. 5A). To corroborate these findings, we measured total cellular porphyrins by LC-qTOF-MS as in Fig. 2; total extracted ion chromatograms are shown in Fig. S6 in the supplemental material. Consistent with the abundance of GtrR, porphyrin intermediates are drastically increased in the $\Delta hemX$ mutant relative to the WT. The $\Delta chdC$ mutant demonstrates intermediate buildup through coproheme because of elevated GtrR levels but is unable to convert coproheme to heme (Fig. 1A). As expected, based on the reduced GtrR abundance shown in Fig. 5A, the porphyrin intermediates are at lower levels in the $\Delta hemX \Delta chdC$ mutant relative to the $\Delta hemX$ or $\Delta chdC$ mutant. These data suggest that heme and HemX do not independently and directly repress GtrR levels, because if so, removal of both would likely have an additive effect on GtrR abundance. Instead the relationship between HemX, heme synthesis, and GtrR levels is still unclear. However, the data are consistent with a model whereby the increase in GtrR levels in heme-deficient strains is dependent on the activity of HemX.

Siroheme synthesis impacts GtrR levels under conditions of nitrite reduction.

The increase in GtrR levels identified in the $\Delta hemX$ mutant likely impacts siroheme synthesis, as the cofactor siroheme is synthesized in *S. aureus* from the shared uroporphyrinogen III intermediate (14) (Fig. 1A). We therefore hypothesized that siroheme levels might also affect GtrR abundance. In the experiments presented thus far, in which *S. aureus* is grown aerobically, siroheme has likely not been synthesized. The siroheme synthesis and siroheme-dependent nitrite reductase genes are transcribed primarily under anaerobic conditions (27). To therefore test the role of siroheme, we first identified conditions under which siroheme synthesis via CysG and siroheme-dependent nitrite reduction by the NirD nitrite reductase were important for growth. As demonstrated in Fig. S7 in the supplemental material, when grown anaerobically, the growth of WT is enhanced when the terminal electron acceptor nitrate is provided. Mutants lacking *cysG* or *nirD* cannot grow to WT levels when nitrate is provided, suggesting that WT cells synthesize siroheme and utilize it in NirD. It is thought that under these conditions, the anaerobic nitrate reductase will reduce nitrate to nitrite, followed by NirD-dependent reduction of nitrite. Deletion of *hemX* does not overtly impact nitrite reduction, as the $\Delta hemX$ strain grows well in nitrate, the $\Delta hemX nirD$ strain phenocopies the *nirD* strain, and the $\Delta hemX cysG$ strain phenocopies the *cysG* strain. Therefore, GtrR abundance was measured by LC-MRM-MS/MS after growth in tryptic soy broth (TSB) containing nitrate (Fig. 6). The strain lacking *cysG*, which can

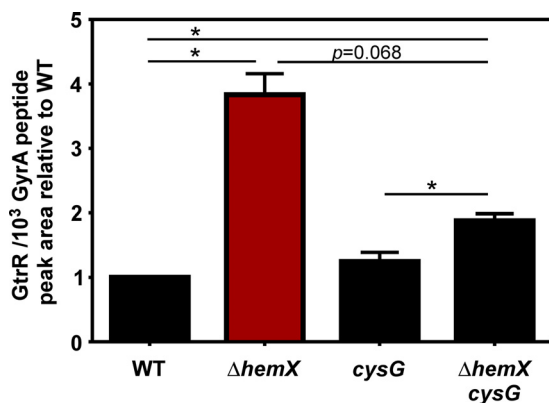


FIG 6 Siroheme synthesis impacts GtrR levels under conditions of nitrite utilization. GtrR was measured by LC-MRM-MS/MS in multiple *S. aureus* strains grown anaerobically with NO₃ provided as the terminal electron acceptor. The data are the average from a single experiment performed in biological triplicate with standard deviation shown. Statistical significance was determined using a one-way ANOVA with Dunnett's correction for multiple comparisons, comparing GtrR abundance for each strain relative to the WT. *, $P < 0.05$.

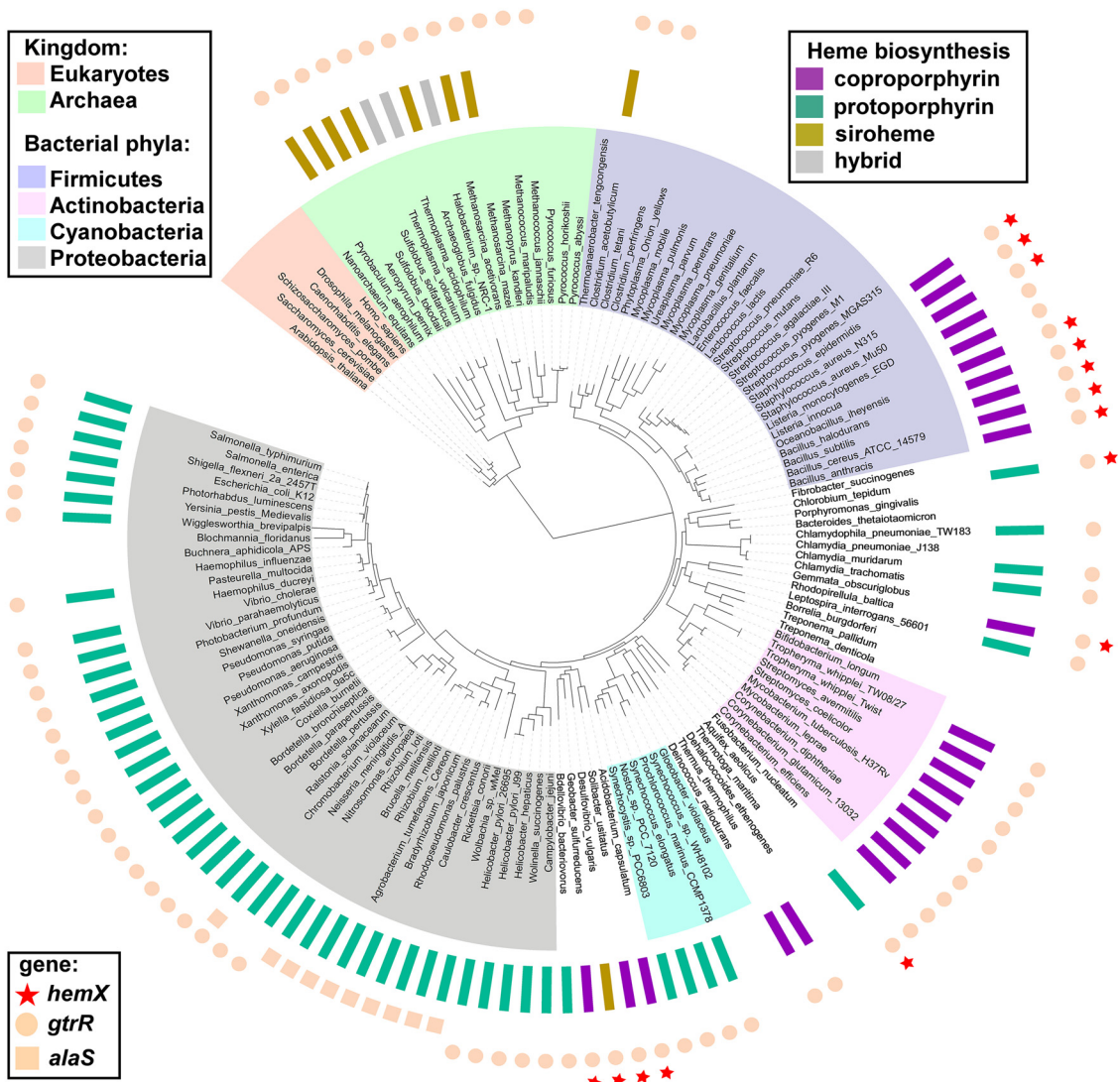
make heme but not siroheme, does not demonstrate elevated GtrR levels. However, the Δ hemX cysG strain has reduced levels compared to the Δ hemX strain, suggesting that siroheme synthesis could impact GtrR regulation.

HemX co-occurs with capacity for heme biosynthesis, and the corresponding genes often colocalize on the chromosome. We hypothesized that *B. subtilis* HemX and *S. aureus* HemX might represent only a subset of HemX homologues that exist across bacterial phyla and function to regulate heme synthesis. Diverse genomes from 978 organisms (924 bacterial and 54 archaeal) were analyzed for the presence of *hemX*. Of these, 113 encode HemX; representative members of this analysis are shown in Fig. 7A. These newly identified homologues expand past the *Bacillales* order, of which representative HemX homologues were previously identified and shown to share function (13). HemX appears to represent an ancient protein family, as it is present in some of the evolutionarily oldest taxa, including *Firmicutes*, *Aquificae*, and *Planctomycetes*. The distribution of *hemX* strongly correlates with the capacity for *de novo* heme synthesis, as *hemX* never occurs in a genome without *gtrR*, and *hemX* never occurs without the capacity for *de novo* heme synthesis. This correlation holds across the microbial kingdom, where *hemX* never occurs in taxa lacking heme biosynthesis genes (within any representatives with sequenced genomes now available): e.g., *Thermotogae*, *Fusobacteria*, and *Mollicutes*. Additionally, the distribution of *hemX* among the members of the *Firmicutes* phylum supports this correlation; *hemX* is present largely in *Bacillales* but does not occur in *Lactobacillales* and only rarely in *Clostridia* (in 2 out of 91 genomes analyzed), which is consistent with the frequent capacity for heme synthesis in *Bacillales* relative to *Lactobacillales* and *Clostridia*. Notably, the genomic co-occurrence of *hemX* and *gtrR* holds true in organisms that synthesize heme via any of the 3 heme biosynthetic pathways identified to date: the coproporphyrin-dependent, siroheme-dependent, or classic protoporphyrin-dependent route (Fig. 7A).

Interestingly, HemX is more commonly found in organisms that encode the ability to synthesize both heme and siroheme (see Fig. S8A in the supplemental material) than in organisms that synthesize heme and not siroheme. This suggests that HemX likely impacts siroheme synthesis as a consequence of affecting GtrR abundance by increasing abundance of uroporphyrinogen III, the final shared biosynthetic intermediate. The co-occurrence of *hemX*, *gtrR*, and *cysG* is also consistent with our findings in Fig. 6 that siroheme synthesis impacts GtrR abundance.

Next we examined the genomic context of *hemX* homologues across 113 organisms carrying *hemX*, as genes associated with the same pathway or area of metabolism tend to colocalize in prokaryotic genomes (28). In 106 (94%) out of these 113 genomes, the

A



B

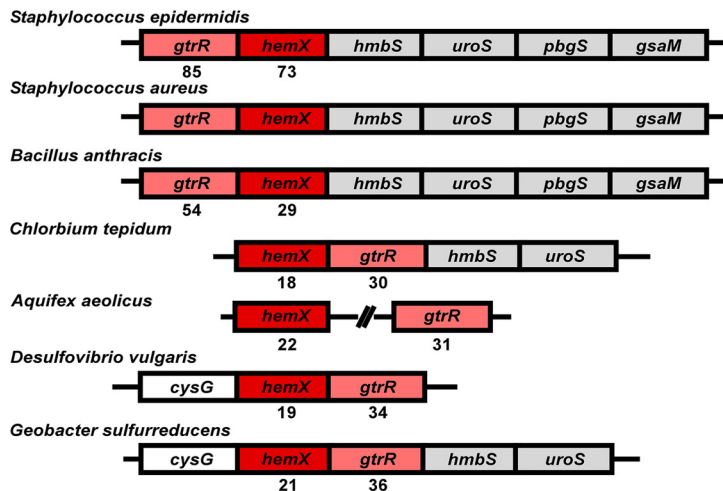


FIG 7 *hemX* is conserved across bacterial phyla and invariably co-occurs (A) and colocalizes (B) with *gtrR*. (A) The occurrence of *hemX* (stars), *gtrR* (circles), and *alaS* (squares) homologues (outermost rings) was mapped onto the tree of life (53). The pathway by which protoheme is synthesized in each of the analyzed organisms is presented in the middle ring as follows (adapted from reference 14): the classic protoporphyrin-dependent pathway (teal), coproporphyrin-dependent path (purple), or siroheme-dependent path (gold). Gray

(Continued on next page)

hemX and *gtrR* genes are adjacent and likely cotranscribed, which is a very strong indicator of their functional association. Seven representatives of these organisms are shown in Fig. 7B, highlighting the common genomic context of *hemX*, *gtrR*, and other genes involved in uroporphyrinogen synthesis (*hmbS*, *uroS*, *pbgS*, and *gsaM*) and siroheme synthesis (*cysG*).

HemX homologues share predicted membrane topology and residues. Comparative genome analysis identified several contextual characteristics of HemX homologues. We therefore investigated the sequences of representative HemX homologues. A multiple-sequence alignment revealed relatively low overall identity among HemX sequences (Fig. 7B); however, the alignment presented in Fig. S8B shows that each HemX homologue shares the same predicted eight-transmembrane-domain topology with N- and C-termini predicted to be extracytoplasmic. Additionally, these divergent homologues share four conserved residues, all in predicted transmembrane domains. Taken together with comparative genome analysis, identification of HemX across bacteria uncovered a strong correlation between *gtrR*, *hemX*, and *de novo* heme synthesis, suggesting that HemX control of GtrR to modulate heme synthesis is a common regulatory strategy among bacteria.

DISCUSSION

In this report, we identify GtrR abundance as a critical regulator of *S. aureus* heme biosynthesis. GtrR catalyzes the initial step in the heme biosynthetic pathway and is maintained at low levels in WT cells proficient for heme biosynthesis, but specifically increases in response to heme deficiency (Fig. 1B). In this study, we used heme auxotrophs to stimulate production of GtrR (Fig. 1D), but we would predict that in particular niches during infection, an increase in heme synthesis is required and GtrR abundance increases to accommodate this need. Host-imposed nitrosative stress, oxidative stress, and hypoxia, for example, all cause *S. aureus* to increase expression of heme-dependent cytochrome oxidases, catalase, and nitric oxide synthase (29–31).

The drastic difference in GtrR enrichment between the heme auxotroph *pbgS* and Δ *chdC* mutants (Fig. 1D and 5A), with deficits in genes at the beginning and end of the heme biosynthetic pathway, respectively, suggests that GtrR abundance during heme deficiency could be impacted by mechanisms other than heme availability. This is an interesting observation in light of the comparative genome analysis of *hemX*, which suggests that HemX could impact siroheme synthesis as well as heme synthesis. It is possible that GtrR abundance is impacted by differences in heme or siroheme abundance as well as abundance in earlier precursor levels, explaining the difference in GtrR levels in the *pbgS* strain relative to the Δ *chdC* strain.

In addition to the impact of heme deficiency on GtrR, we also identify HemX as a key regulator of GtrR in heme-proficient cells (Fig. 2A). Our broad genomic analysis has identified HemX homologues across bacterial phyla, suggesting that HemX control of heme synthesis via GtrR is a conserved strategy (Fig. 7; Fig. S8). This finding is consistent with the model set forth by Hederstedt and colleagues (18, 21); in both *B. subtilis* and now *S. aureus*, it appears that HemX regulates GtrR abundance posttranscriptionally (Fig. 2B) through an as-yet-undefined mechanism. *B. subtilis* HemX is sufficient to affect GtrR abundance when both are expressed ectopically in *Escherichia coli* (18); however, the contribution of heme or conserved *E. coli* proteins in this system is unclear, making it challenging to conclude if HemX directly interacts with GtrR. Together, our findings are consistent with a model whereby GtrR is regulated by heme abundance and HemX through a multiprotein mechanism. Our finding that GtrR abundance is reduced in the

FIG 7 Legend (Continued)

rectangles mark the organisms that contain unusual combinations of genes normally involved in different pathways for protoheme synthesis (hybrid paths [14]). The absence of a rectangle in the middle ring indicates the absence of any known route for protoheme synthesis in an organism. Likewise, the absence of a circle (*gtrR*) or square (*alaS*) in the outermost ring shows the inability of an organism to produce tetrapyrroles of any kind. Note that *hemX* does not occur in such organisms. (B) The immediate genomic neighborhood of the *hemX* gene in seven representative genomes, with ClustalW alignment scores for HemX and GtrR for each organism relative to *S. aureus*.

$\Delta hemX$ *pbgS* strain relative to the *pbgS* strain and not increased supports this model: heme and HemX both do not directly repress GtrR levels (Fig. 5A). In *Salmonella* strains, which do not encode HemX, GtrR is regulated by N-terminal proteolysis by ClpAP and Lon proteases to keep levels low (32). Additionally, *Salmonella* GtrR binds excess heme through a Cys-170 residue (33). Mutagenesis of the N-terminus degradation sequence or heme binding cysteine disrupts regulation, and it has been proposed that heme-bound GtrR but not apo-GtrR is a substrate for the proteases (32, 34). The mechanism by which *Salmonella* GtrR is regulated by proteases via its N terminus and heme binding is not fully understood, and these regulatory amino acids are not conserved in *S. aureus* GtrR. Likewise, further work is needed to dissect the unique regulatory effects of heme and HemX on GtrR levels and the potential involvement of proteolysis in this process in *S. aureus*.

In the absence of HemX, *S. aureus* synthesizes excess heme. The increase in heme synthesis disrupts intracellular iron homeostasis (Fig. 4), which could additionally disrupt the expression of the staphyloferrin B siderophore biosynthetic genes, which were recently identified to be under the control of a transcriptional activator that is inactive when bound to heme (35). This altered iron homeostasis would likely reduce the function of many important Fe-S cluster-containing enzymes critical to staphylococcal physiology. Additionally, excess heme synthesized in the $\Delta hemX$ mutant activates the heme stress response (Fig. 3). While activation of the HssRS two-component system was first recognized as the result of exogenous heme, our findings add to a growing body of literature that supports a model whereby endogenous heme and exogenous heme both contribute to HssRS activation and heme toxicity. We have previously identified small molecule activators of heme synthesis that increase intracellular heme and activate HssRS (36–38), adding to our genetic evidence presented in this work that endogenous heme activates HssRS. Here, the increase in endogenous heme in the $\Delta hemX$ mutant is not toxic because of the HssRS-HrtAB detoxification response. Rather, endogenous heme activation of HssRS provides resistance to heme toxicity through preadaptation and expression of *hrtAB* (Fig. 3C and D). The impact of inactivation of *hemX* on the fitness of pathogens that do not encode the HssRS-HrtAB system would offer insight into whether dysregulated heme synthesis is sufficient to induce heme toxicity from within.

This study found that regulation of GtrR abundance is sufficient to regulate total heme synthesis (Fig. 2), consistent with multiple reports that ALA formation is a critical rate-limiting step in heme synthesis (14). Indeed, regulation of ALA synthesis via control of either GtrR or ALAS has emerged as a theme across kingdoms. In metazoans, two ALAS isoforms exist and are impacted by heme (reviewed in reference 39). In the plant model organism *Arabidopsis thaliana*, ALA synthesis is regulated by degradation of GluTR via Clp proteolysis from the N terminus as well as stabilization and activation of a regulatory binding protein (40, 41). In Gram-negative model organisms, as mentioned above, GtrR abundance is regulated by heme and proteolysis (32). Our findings extend this paradigm further into the *Firmicutes* phylum of bacteria.

The specific mechanism by which HemX impacts GtrR abundance remains undefined. HemX is annotated as a member of the cytochrome *c* assembly protein family (Pfam accession no. PF01578), suggesting that it may be involved in heme binding and trafficking at the membrane. However, *S. aureus* does not encode *c*-type cytochromes. The capacity of HemX to bind heme has not been experimentally validated, but excess heme does accumulate in the membrane (42), which is suggestive of a potential role for membrane-localized heme reservoirs or chaperones. The limited regions of HemX predicted to be cytoplasmic suggest that protein-protein interactions likely occur between other membrane proteins, but no HemX-interacting partners have been identified to date. Additionally, GtrR residues that impact regulation by either heme or HemX are unknown, but would offer information as to the regulatory steps between heme, HemX, and GtrR, which appear to be complex. Although heme-dependent inhibition of *S. aureus* heme synthesis was first proposed in 1962 (43), the impact of HemX and heme on GtrR abundance continues to warrant further investigation.

TABLE 1 *S. aureus* strains used in this study

Strain	Genotype	Description	Source or reference
Newman	WT	Wild-type, methicillin-sensitive clinical isolate	57
Newman	<i>pbgS</i>	<i>pbgS</i> (NWMN_1562) gene interrupted with erythromycin resistance gene <i>ermB</i> by homologous recombination, transduced into Newman	3
Newman	$\Delta chdC$	In-frame unmarked deletion of <i>chdC</i> (NWMN_0550) generated by allelic exchange	58
Newman	$\Delta hemX \Delta chdC$	In-frame unmarked deletion of <i>chdC</i> (NWMN_0550) generated by allelic exchange in $\Delta hemX$ strain	This work
Newman	$\Delta menB$	In-frame unmarked deletion of <i>menB</i> generated by allelic exchange	59
Newman	$\Delta qoxB \text{ } cydB$	In-frame unmarked deletion of <i>qoxB</i> and <i>cydB</i> ::Tn	3
JE2	<i>katA</i>	<i>katA</i> ::Tn (NE1366)	BEI (46)
Newman	<i>katA</i>	<i>katA</i> ::Tn (NE1366), transduced into Newman	This work
Newman	$\Delta hemX$	In-frame unmarked deletion of <i>hemX</i> (NWMN_1565)	This work
RN9011		RN4220 carrying pRN7023 integrase plasmid	24
RN9011	<i>attC</i> :: P_{Igt}	pJC1111 P_{Igt} integrated into chromosome at <i>attC</i> locus	This work
RN9011	<i>attC</i> :: $P_{Igt}hemX$	pJC1111 $P_{Igt}hemX$ integrated into chromosome at <i>attC</i> locus	This work
Newman	$\Delta hemX \text{ } attC$:: P_{Igt}	pJC1111 P_{Igt} integrated into chromosome at <i>attC</i> locus	This work
Newman	$\Delta hemX \text{ } attC$:: $P_{Igt}hemX$	pJC1111 $P_{Igt}hemX$ integrated into chromosome at <i>attC</i> locus	This work
Newman	<i>attC</i> :: P_{Igt}	pJC1111 P_{Igt} integrated into chromosome at <i>attC</i> locus	This work
Newman	$\Delta hemX \text{ } pbgS$	In-frame unmarked deletion of <i>hemX</i> (NWMN_1565) in <i>pbgS</i> strain	This work
Newman	$\Delta hssRS$	In-frame unmarked deletion of <i>hssRS</i> generated by allelic exchange	60
Newman	$\Delta hrtB$	In-frame unmarked deletion of <i>hrtB</i> generated by allelic exchange	61
Newman	<i>hrtB</i>	<i>hrtB</i> ::Tn(PhiNE01762)	10
Newman	$\Delta hemX \text{ } hrtB$	<i>hrtB</i> ::Tn(PhiNE01762) allele transduced to $\Delta hemX$ strain	This work
JE2	<i>cysG</i>	<i>cysG</i> ::Tn (NE1931; SAUSA300_2553::Tn)	BEI (46)
Newman	<i>cysG</i>	<i>cysG</i> ::Tn (NE1931) transduced into Newman	This work
Newman	$\Delta hemX \text{ } cysG$	<i>cysG</i> ::Tn (NE1931) transduced into Newman $\Delta hemX$	This work
JE2	<i>nirD</i>	<i>nirD</i> ::Tn (NE1279)	BEI (46)
Newman	<i>nirD</i>	<i>nirD</i> ::Tn (NE1279) transduced into Newman	This work
Newman	$\Delta hemX \text{ } nirD$	<i>nirD</i> ::Tn (NE1279) transduced into Newman $\Delta hemX$	This work
Newman	$\Delta gtrR \text{ } hemX$	In-frame unmarked deletion of <i>gtrR</i> and <i>hemX</i> (NWMN_1565-1566) generated by single allelic exchange	This work
RN4220		Restriction-deficient cloning intermediate strain	62

MATERIALS AND METHODS

Bacterial strains and reagents. Bacterial strains (Table 1), plasmids (see Table S1 in the supplemental material), and primers (Table S1) are listed in the specified table. *S. aureus* strains were grown routinely on tryptic soy agar (TSA) or broth (TSB) supplemented with 10 $\mu\text{g/ml}$ chloramphenicol or 10 $\mu\text{g/ml}$ erythromycin when necessary. When used, heme (hemin chloride) was used at the concentrations noted. Heme was prepared fresh at 10 mM in 0.1 M NaOH; for experiments in which heme was used, an equal volume of 0.1 M NaOH was used for all conditions. *E. coli* strains were grown on lysogeny broth (LB) or LB agar (LBA), supplemented with 50 $\mu\text{g/ml}$ carbenicillin when necessary. For growth in liquid medium, an Innova44 incubator shaking at 180 rpm was used. For standard cultures of 4 to 5 ml, 15-ml round-bottomed polypropylene tubes with aeration lids were used, at a 45° angle in the incubator. For cloning and mutagenesis in plasmids, all constructs were confirmed by sequencing (GeneWiz). Unless noted otherwise, all chemicals are from Sigma. All molecular biology reagents were from New England Biolabs (NEB) and used according to the manufacturer's instructions, unless otherwise noted. Phusion 2X Hi-fidelity master mix was used for all PCRs for cloning. As necessary, plasmids were transformed by electroporation from *E. coli* into the *S. aureus* cloning intermediate strain RN4220 before isolation and subsequent electroporation into the final *S. aureus* strains.

(i) Deletion of genes by allelic exchange. Deletion of *hemX* and *chdC* was performed by allelic exchange as described in reference 44 with some modifications. The pKOR1 plasmids containing ~1-kb homologous regions flanking upstream and downstream of the gene to be deleted were prepared using NEB Hi-Fi assembly according to manufacturer's suggestions. The pKOR1 backbone was amplified by PCR using JC291/292, which produces a linear product not including the *attB* recombination sites. The ~1-kb flanking regions were amplified from the *S. aureus* Newman genomic DNA. Deletions were confirmed by PCR using isolated genomic DNA and complemented by providing the gene in *cis* or *trans*. Additional details are found in Text S1 in the supplemental material.

(ii) *hemX* chromosomal integration. Chromosomal complementation was performed by cloning P_{Igt} or $P_{Igt}hemX$ into pJC1111. P_{Igt} was PCR amplified from pOS1 P_{Igt} using JC158/229 and subsequently cloned into the multiple cloning site of pJC1111 after restriction digestion with Sall and BamHI. *hemX* was cloned into pOS1 P_{Igt} by amplifying *hemX* flanked by NdeI and BamHI sites from *S. aureus* Newman genomic DNA using primers JC157/155 and ligated (T4 ligase) into the multiple cloning site of pOS1 P_{Igt} after restriction digestion with NdeI and BamHI. $P_{Igt}hemX$ was amplified from pOS1 $P_{Igt}hemX$ using

JC158/155 and subsequently cloned into the Sall and BamHI sites of pJC1111 after restriction digestion with Sall and BamHI. pJC1111 P_{igt} and pJC1111 P_{igt} *hemX* were integrated into the chromosome of strain RN9011 as described previously (24) and then transduced into the *S. aureus* Newman WT or Δ *hemX* mutant as noted. Transductions of pJC1111 loci were performed with ϕ 85 as described in reference 45, with some modifications: after incubation of donor phage with recipient strains and washing with sodium citrate, cells were allowed to recover for 4 h in TSB with 40 mM sodium citrate at 37°C with shaking and plated to TSA containing 0.15 mM cadmium chloride.

(iii) Transduction of transposon library alleles. For transduction of transposon library alleles, the *katA::Tn* (NE1366), *cysG::Tn* (NE1931), *nirD::Tn* (NE1279), and *hrtB::Tn* (PhiNE01762) transposon alleles were transduced to the *S. aureus* Newman and Δ *hemX* strains as listed in Table 1 as described previously (45) using bacteriophage ϕ 85; alleles were confirmed by an inverse-PCR method and Sanger sequencing (46).

Catalase activity. To assess catalase activity, strains were grown for 16 h in TSB, and then 50 μ l of each culture was spotted onto a TSA plate and streaked for isolation. After 24 h of growth at 37°C, 50 μ l of 30% H₂O₂ was added to each strain and immediately imaged.

LC-MRM-MS/MS. Strains were streaked onto TSA and grown for 24 h at 37°C. Cultures were started from single colonies in 5 ml of RPMI plus 1% Casamino Acids and grown at 37°C for 15 h. Overnight cultures were subcultured 1:100 into RPMI plus 1% Casamino Acids and grown until mid-exponential phase. For small-colony variants without chemical complementation, overnight cultures were subcultured 1:25. For conditions under which heme was added, 2 μ M was used; for menaquinone, 12.5 μ M menaquinone-vitamin K₂ was used.

For anaerobic experiments, a Coy (Grass Lake, MI) anaerobic chamber was used, filled with a mixture of 90% nitrogen, 5% carbon dioxide, and 5% hydrogen gases, and hydrogen levels were monitored to ensure a minimum 2% hydrogen concentration. Palladium catalysts (Coy) were used to remove any residual oxygen by reaction with hydrogen. A Coy static incubator was maintained at 37°C. Solutions and plasticware were allowed to equilibrate for >24 h inside the glove box before use. For anaerobic samples, strains were streaked onto TSA and grown aerobically for 24 h at 37°C. Cultures were started from single colonies in 5 ml of anaerobic TSB and grown at 37°C for 15 h. Overnight cultures were subcultured 1:100 into anaerobic TSB containing 40 mM sodium nitrate and grown until the mid-exponential phase. Protein was collected, tryptically digested, and subjected to LC-MRM-MS/MS as described in Text S1 in the supplemental material.

Anaerobic growth curves. The *S. aureus* Newman WT, Δ *hemX*, *cysG*, Δ *hemX cysG*, *nirD*, and Δ *hemX nirD* strains were streaked onto TSA and grown aerobically for 24 h at 37°C. Cultures were started from single colonies in 3 ml of anaerobic TSB and grown at 37°C for 15 h. Overnight cultures were subcultured 1:200 in round-bottomed 96-well plates with 200 μ l of anaerobic TSB containing 40 mM sodium nitrate or an equal volume of sterile water and covered with Breathe-Easy gas-permeable seal (Sigma). Growth was monitored by optical density (OD) over time in a BioTek Synergy H1.

Quantitative reverse transcriptase PCR. Strains were streaked onto TSA and grown at 24 h at 37°C. Cultures were started from single colonies in 5 ml of RPMI plus 1% Casamino Acids and grown at 37°C for 15 h. Overnight cultures were subcultured 1:100 (WT and Δ *hemX* mutant) or 1:25 (*pbgS* Δ *hemX pgbS* strain) into RPMI plus 1% Casamino acids and grown until the mid-exponential phase. An equal volume of ice-cold acetone-ethanol was added, and the mixture was stored at -80°C. RNA was isolated using Tri reagent and chloroform and precipitated with isopropanol. Isolated RNAs were treated with DNase I (Thermo) according to the manufacturer's instructions, and RNA was reisolated using Qiagen RNeasy kit. cDNA was synthesized from 2 μ g of RNA by incubation with Moloney murine leukemia virus (MMLV) reverse transcriptase (Thermo), using transcript-specific primers (JC83/84 for *gyrA*, JC53/54 for *gtrR*, and JC55/56 for *gsaM*). Quantitative PCR (qPCR) was performed using SYBR green (Thermo) according to the manufacturer's instructions, using primers JC81/82 for *gyrA*, HS1/2 for *gtrR*, and HS for *gsaM*. Transcript abundance was quantified using the threshold cycle ($\Delta\Delta C_t$) method after normalization to *gyrA* abundance.

ALA quantification. ALA quantification was modified from reference 47. The *S. aureus* WT and Δ *hemX* mutant strains were streaked onto TSA and grown for 18 h at 37°C. Single colonies were used to start 5-ml cultures in TSB and grown for 12 h at 37°C, then 1 ml was inoculated into 100 ml of TSB in a 250-ml Erlenmeyer flask and grown at 37°C for 14 h. The cell wall was removed by incubation in TSM (100 mM Tris-Cl, pH 7, 500 mM sucrose, 10 mM MgCl₂) plus 40 μ g/ml lysostaphin and incubated at 37°C for 45 min. Protoplasts were collected by centrifugation and resuspended in 1 ml 10% trichloroacetic acid (TCA). Samples were incubated on ice and intermittently lysed by sonication. The soluble fraction was collected by centrifugation and neutralized to pH 7 with 6 M NaOH, then added to a Dowex 1x-4 resin in column converted to the acetate form before use. In this form, the column retains porphobilinogen but allows ALA to flow through. Six hundred microliters of flowthrough was added to 200 μ l of 8% acetyl acetone in 2 M sodium acetate buffer, incubated for 15 min at 90°C to form the pyrrolic condensation product, and cooled to room temperature. Five hundred microliters of sample was added to 500 μ l of modified Ehrlich's reagent and incubated for 10 min at room temperature, and the resulting absorbance was measured at 552 and 650 nm in a Cary 50 Bio UV-visible (UV-Vis) spectrophotometer. The relative concentration of ALA was calculated based on an extinction coefficient of $7.2 \times 10^{-4} \text{ M}^{-1} \text{ cm}^{-1}$.

LC-qTOF-MS porphyrin quantification. Porphyrins were extracted from the *S. aureus* WT and Δ *hemX* strains grown to the stationary phase and analyzed by LC-qTOF-MS described in detail in Text S1 in the supplemental material.

Pyridine hemochromagen quantification. Strains were streaked onto TSA and grown for 18 h at 37°C. Single colonies were used to start 5-ml cultures of TSB and grown at 37°C for 10 h. Sixty microliters of each culture was added to 6 ml of TSB and grown for 16 h at 37°C. Cells were collected by

centrifugation, and the cell wall was removed by incubation in 20 mM potassium phosphate buffer (pH 7.4) containing 20 μg of lysostaphin for 45 min at 37°C. Samples were lysed by sonication, and unbroken cells were collected by centrifugation. Four hundred fifty microliters of the soluble supernatant was added to 450 μl of 0.2 M NaOH containing 40% pyridine and 500 μM potassium ferricyanide. Absorbance was measured in a Cary 50 Bio UV-Vis spectrophotometer from 540 to 590 nm. Ten microliters of 0.5 M sodium dithionite prepared in 0.5 M NaOH was added to samples, the mixture was incubated for 5 min, and absorbance (A) was measured again from 540 to 590 nm. Heme quantity is calculated using $\Delta A = (A_{557 \text{ reduced}} - A_{557 \text{ oxidized}}) - (A_{575 \text{ reduced}} - A_{575 \text{ oxidized}})$ and an extinction coefficient of 32.4 $\text{mM}^{-1} \text{cm}^{-1}$.

Bioluminescent reporter assay. The *S. aureus* WT and ΔhemX strain with pXen-1 or $P_{\text{hrt}}\text{luxABCDE}$ were streaked onto TSA-chloramphenicol prepared with 0 or 20 μM heme. After 18 h, the plates were imaged using a Xenogen IVIS 2000.

XylE reporter assay. XylE abundance in cellular lysate was assessed spectrophotometrically by measuring formation of 2-hydroxymuconic acid from catechol after growth in TSB containing chloramphenicol and 0 to 2 μM heme, as described previously (10).

Heme killing assay. *S. aureus* WT, ΔhemX , and ΔhrtB strains were streaked onto TSA and grown for 24 h at 37°C. Single colonies were used to start 5-ml cultures of TSB and grown at 37°C for 14 h. Two microliters of each culture was added to 148 μl of TSB containing different concentrations of heme in a 96-well round-bottomed plate and incubated at 37°C for 2 h. Samples were serially diluted in phosphate-buffered saline (PBS) and plated to TSA for CFU enumeration after 24 h of growth at 37°C.

Heme toxicity growth curves. Strains were streaked onto TSA and grown for 24 h at 37°C. Single colonies were used to start 5 ml cultures of TSB and grown for 16 h at 37°C containing 0 or 2 μM heme as noted. One microliter of each culture was added to 199 μl of medium containing 0 or 10 μM heme, as noted, in a 96-well round-bottomed plate, and growth was monitored over time at 37°C by measuring the optical density at 600 nm (OD_{600}) in a BioTek Synergy2 spectrophotometer and analyzed with BioTek Gen5 software.

Growth in minimal medium. Chemically defined media (CDM) supplemented with 5 mg/ml glucose was prepared as previously described (48), with the exception that iron was not added. Strains were streaked onto TSA and grown for 24 h at 37°C. Single colonies were used to start 5-ml cultures in TSB and grown for 14 h at 37°C. Cells were collected by centrifugation, washed in PBS twice, and then resuspended in 5 ml of PBS. One microliter was added to 199 μl of CDM containing 1 μM ethylenediamine-*N,N'*-bis(2-hydroxyphenylacetic acid) (EDDHA; LGC Standards) or an equal volume of 0.1 M NaOH (vehicle) in a 96-well round-bottomed plate. Growth was monitored for 24 h with shaking at 37°C in a BioTek EPOCH2 spectrophotometer and analyzed with BioTek Gen5 software.

pOS1 P_{isdA} gfp reporter assay. The *S. aureus* WT pOS1 P_{isdA} gfp and ΔhemX pOS1 P_{isdA} gfp strains were streaked onto TSA-chloramphenicol and grown for 14 h at 37°C. Single colonies were used to inoculate 5-ml cultures of TSB-chloramphenicol and grown at 37°C for 8.5 h. One microliter of each culture was used to inoculate 199 μl of TSB-chloramphenicol containing 1 mM 2,2-dipyridyl or an equal volume of ethanol (vehicle). Growth was monitored over the course of 16 h by measuring OD_{600} as well as relative fluorescence at 485 nm (excitation) and 510 nm (emission) in a BioTek Cytation5 spectrophotometer and analyzed with BioTek Gen5 software.

Comparative genome analysis. With over 100,000 prokaryotic genomes currently available in public databases and many more in the pipelines (<http://www.genomesonline.org>), it is not practical or possible to perform meaningful comparative analysis on all of them simultaneously. Thus, a set of diverse representative prokaryotic genomes have been developed in the SEED database as follows. The algorithm for computing molecular operational taxonomic units (OTU) based on DNA barcode data (49, 50) was used to group ~12,600 prokaryotic genomes available in the SEED database in October 2013 into about 1,000 taxon groups. One or two representative genomes (rarely three) for each OTU were selected based on the largest amount of published experimental data and the highest level of research interest within the scientific community. The resultant collection of 982 diverse genomes (928 eubacterial and 54 archaeal) creates a manageable set that accurately represents the immense diversity of the over 12,000 prokaryotic organisms with sequenced genomes. Importantly, it is not skewed by an overabundance of genomes for a few microbial genera (medically or industrially important), such as *Enterobacteriaceae*, streptococci, mycobacteria, etc.

The HemX protein family was exhaustively annotated for this set of 982 representative microbial genomes in the SEED database (51). Contextual associations for this family were predicted based on the patterns of co-occurrence and/or colocalization of its members with other protein families using the set of tools for comparative genome analysis available in SEED (52) within the functional and genomic contexts provided by the subsystem "Heme Biosynthesis: protoporphyrin-, coproporphyrin- and siroheme-dependent pathways" (http://pubseed.theseed.org/SubsysEditor.cgi?page=ShowSubsystem&subsystem=Heme_Biosynthesis%3A_protoporphylin-%2C_coproporphyrin-_and_siroheme-dependent_pathways). Phylogenetic distribution of the HemX protein family was mapped onto the tree of life (53), and protoheme biosynthetic pathway analysis was adapted from reference 14.

HemX multiple sequence alignment and topology prediction. The HemX multiple sequence alignment was KEGG ClustalW (<http://www.genome.jp> [accessed March 2017]) (54) using *Staphylococcus aureus* strain Newman, *Staphylococcus epidermidis* strain ATCC 12228, *Bacillus anthracis* strain Sterne, *Chlorobium tepidum* strain TLS, *Aquifex aeolicus* strain VF5, *Desulfovibrio vulgaris* strain DP4, and *Geobacter sulfurreducens* strain PCA. The transmembrane domains depicted were predicted by MEMSAT3 (<http://bioinf.cs.ucl.ac.uk>; accessed March 2017) as described previously (55). All models were confirmed using TMHMM 2.0 (<http://www.cbs.dtu.dk> [accessed March 2017]) (56), and predictions were matched

across prediction servers, with the exception of *Chlorobium tepidum*, which TMHMM2.0 predicts to have seven rather than eight transmembrane domains.

Statistical analysis. All data analysis and statistical tests were performed using GraphPad Prism 6 software. Replicate numbers and statistical tests for each experiment are listed in the figure legends.

SUPPLEMENTAL MATERIAL

Supplemental material for this article may be found at <https://doi.org/10.1128/mBio.02287-17>.

TEXT S1, DOCX file, 0.1 MB.

FIG S1, TIF file, 0.9 MB.

FIG S2, TIF file, 0.3 MB.

FIG S3, TIF file, 2.7 MB.

FIG S4, TIF file, 6.8 MB.

FIG S5, TIF file, 0.7 MB.

FIG S6, TIF file, 3.1 MB.

FIG S7, TIF file, 4.1 MB.

FIG S8, TIF file, 45.3 MB.

TABLE S1, DOCX file, 0.1 MB.

ACKNOWLEDGMENTS

We thank Lars Hederstedt (Lund University) and members of the Skaar laboratory for their critical evaluation of the manuscript. We thank Victor Torres (New York University) for the gift of strains and plasmids. We thank Neal Hammer and Matt Surdel for transduction of *katA::Tn* and *nirD::Tn*, respectively. We thank Hayes McDonald and the Vanderbilt Mass Spectrometry Research Core for assistance with mass spectrometry experiments. Strains NE1279, NE1366, and NE1931 were obtained through the Network on Antimicrobial Resistance in *Staphylococcus aureus* (NARSA) for distribution by BEI Resources, NIAID, NIH (Nebraska Transposon Mutant Library [NTML] Screening Array, NR-48501).

This work was funded by National Institutes of Health F31AI126662 (J.E.C.), T32GM065086 (J.E.C.), T32HL094296 (C.M.G.), R01AI0690233 (E.P.S.), R01GM090260 (J.L.D.), and R21DK114607 (J.L.D.).

The funders had no role in study design, data collection and interpretation, or the decision to submit the work for publication.

REFERENCES

- Choby JE, Skaar EP. 2016. Heme synthesis and acquisition in bacterial pathogens. *J Mol Biol* 428:3408–3428. <https://doi.org/10.1016/j.jmb.2016.03.018>.
- Klevens RM, Morrison MA, Nadle J, Petit S, Gershman K, Ray S, Harrison LH, Lynfield R, Dumyati G, Townes JM, Craig AS, Zell ER, Fosheim GE, McDougal LK, Carey RB, Fridkin SK, Active Bacterial Core surveillance (ABCs) MRSA Investigators. 2007. Invasive methicillin-resistant *Staphylococcus aureus* infections in the United States. *JAMA* 298:1763–1771. <https://doi.org/10.1001/jama.298.15.1763>.
- Hammer ND, Reniere ML, Cassat JE, Zhang Y, Hirsch AO, Hood MI, Skaar EP. 2013. Two heme-dependent terminal oxidases power *Staphylococcus aureus* organ-specific colonization of the vertebrate host. *mBio* 4:e00241–13. <https://doi.org/10.1128/mBio.00241-13>.
- Hammer ND, Schurig-Briccio LA, Gerdes SY, Gennis RB, Skaar EP. 2016. CtaM is required for menaquinol oxidase aa3 function in *Staphylococcus aureus*. *mBio* 7:e00823–16. <https://doi.org/10.1128/mBio.00823-16>.
- Dailey HA, Gerdes S, Dailey TA, Burch JS, Phillips JD. 2015. Noncanonical coproporphyrin-dependent bacterial heme biosynthesis pathway that does not use protoporphyrin. *Proc Natl Acad Sci U S A* 112:2210–2215. <https://doi.org/10.1073/pnas.1416285112>.
- Lobo SA, Scott A, Videira MA, Winpenny D, Gardner M, Palmer MJ, Schroeder S, Lawrence AD, Parkinson T, Warren MJ, Saraiva LM. 2015. *Staphylococcus aureus* haem biosynthesis: characterisation of the enzymes involved in final steps of the pathway. *Mol Microbiol* 97:472–487. <https://doi.org/10.1111/mmi.13041>.
- Cosgrove K, Coutts G, Jonsson IM, Tarkowski A, Kokai-Kun JF, Mond JJ, Foster SJ. 2007. Catalase (KatA) and alkyl hydroperoxide reductase (AhpC) have compensatory roles in peroxide stress resistance and are required for survival, persistence, and nasal colonization in *Staphylococcus aureus*. *J Bacteriol* 189:1025–1035. <https://doi.org/10.1128/JB.01524-06>.
- van Sorge NM, Beasley FC, Gusarov I, Gonzalez DJ, von Köckritz-Blickwede M, Anik S, Borkowski AW, Dorrestein PC, Nudler E, Nizet V. 2013. Methicillin-resistant *Staphylococcus aureus* bacterial nitric oxide synthase affects antibiotic sensitivity and skin abscess development. *J Biol Chem* 288:6417–6426. <https://doi.org/10.1074/jbc.M112.448738>.
- Mogen AB, Carroll RK, James KL, Lima G, Silva D, Culver JA, Petucci C, Shaw LN, Rice KC. 2017. *Staphylococcus aureus* nitric oxide synthase (saNOS) modulates aerobic respiratory metabolism and cell physiology. *Mol Microbiol* 105:139–157. <https://doi.org/10.1111/mmi.13693>.
- Torres VJ, Stauff DL, Pishchany G, Bezbradica JS, Gordy LE, Iturregui J, Anderson KL, Dunman PM, Joyce S, Skaar EP. 2007. A *Staphylococcus aureus* regulatory system that responds to host heme and modulates virulence. *Cell Host Microbe* 1:109–119. <https://doi.org/10.1016/j.chom.2007.03.001>.
- Beale SI, Castelfranco PA. 1973. ¹⁴C incorporation from exogenous compounds into δ -aminolevulinic acid by greening cucumber cotyledons. *Biochem Biophys Res Commun* 52:143–149. [https://doi.org/10.1016/0006-291X\(73\)90966-2](https://doi.org/10.1016/0006-291X(73)90966-2).
- Schön A, Krupp G, Gough S, Berry-Lowe S, Kannangara CG, Söll D. 1986. The RNA required in the first step of chlorophyll biosynthesis is a

- chloroplast glutamate tRNA. *Nature* 322:281–284. <https://doi.org/10.1038/322281a0>.
13. Moser J, Schubert WD, Beier V, Bringemeier I, Jahn D, Heinz DW. 2001. V-shaped structure of glutamyl-tRNA reductase, the first enzyme of tRNA-dependent tetrapyrrole biosynthesis. *EMBO J* 20:6583–6590. <https://doi.org/10.1093/emboj/20.23.6583>.
 14. Dailey HA, Dailey TA, Gerdes S, Jahn D, Jahn M, O'Brian MR, Warren MJ. 2017. Prokaryotic heme biosynthesis: multiple pathways to a common essential product. *Microbiol Mol Biol Rev* 81:81:e00048-16. <https://doi.org/10.1128/MMBR.00048-16>.
 15. Hansson M, Gustafsson MC, Kannangara CG, Hederstedt L. 1997. Isolated *Bacillus subtilis* HemY has coproporphyrinogen III to coproporphyrin III oxidase activity. *Biochim Biophys Acta* 1340:97–104. [https://doi.org/10.1016/S0167-4838\(97\)00030-7](https://doi.org/10.1016/S0167-4838(97)00030-7).
 16. Gerber SA, Rush J, Stemman O, Kirschner MW, Gygi SP. 2003. Absolute quantification of proteins and phosphoproteins from cell lysates by tandem MS. *Proc Natl Acad Sci U S A* 100:6940–6945. <https://doi.org/10.1073/pnas.0832254100>.
 17. Proctor RA, von Eiff C, Kahl BC, Becker K, McNamara P, Herrmann M, Peters G. 2006. Small colony variants: a pathogenic form of bacteria that facilitates persistent and recurrent infections. *Nat Rev Microbiol* 4:295–305. <https://doi.org/10.1038/nrmicro1384>.
 18. Schröder I, Johansson P, Rutberg L, Hederstedt L. 1994. The *hemX* gene of the *Bacillus subtilis* *hemAXCDBL* operon encodes a membrane protein, negatively affecting the steady-state cellular concentration of HemA (glutamyl-tRNA reductase). *Microbiology* 140:731–740. <https://doi.org/10.1099/00221287-140-4-731>.
 19. Wang LY, Brown L, Elliott M, Elliott T. 1997. Regulation of heme biosynthesis in *Salmonella typhimurium*: activity of glutamyl-tRNA reductase (HemA) is greatly elevated during heme limitation by a mechanism which increases abundance of the protein. *J Bacteriol* 179:2907–2914. <https://doi.org/10.1128/jb.179.9.2907-2914.1997>.
 20. Bibb LA, Kunkle CA, Schmitt MP. 2007. The ChrA-ChrS and HrrA-HrrS signal transduction systems are required for activation of the *hmuO* promoter and repression of the *hemA* promoter in *Corynebacterium diphtheriae*. *Infect Immun* 75:2421–2431. <https://doi.org/10.1128/IAI.01821-06>.
 21. Johansson P, Hederstedt L. 1999. Organization of genes for tetrapyrrole biosynthesis in Gram-positive bacteria. *Microbiology* 145:529–538. <https://doi.org/10.1099/13500872-145-3-529>.
 22. Hansson M, Rutberg L, Schröder I, Hederstedt L. 1991. The *Bacillus subtilis* *hemAXCDBL* gene cluster, which encodes enzymes of the biosynthetic pathway from glutamate to uroporphyrinogen III. *J Bacteriol* 173:2590–2599. <https://doi.org/10.1128/jb.173.8.2590-2599.1991>.
 23. Schröder I, Hederstedt L, Kannangara CG, Gough P. 1992. Glutamyl-tRNA reductase activity in *Bacillus subtilis* is dependent on the *hemA* gene product. *Biochem J* 281:843–850. <https://doi.org/10.1042/bj2810843>.
 24. Chen J, Yoong P, Ram G, Torres VJ, Novick RP. 2014. Single-copy vectors for integration at the SaP11 attachment site for *Staphylococcus aureus*. *Plasmid* 76:1–7. <https://doi.org/10.1016/j.plasmid.2014.08.001>.
 25. Hooper JK, Kahn A, Ash DE, Gough S, Kannangara CG. 1988. Biosynthesis of delta-aminolevulinic acid in greening barley leaves. IX. Structure of the substrate, mode of gabaculine inhibition, and the catalytic mechanism of glutamate 1-semialdehyde aminotransferase. *Carlsberg Res Commun* 53:11–25. <https://doi.org/10.1007/BF02908411>.
 26. Mazmanian SK, Skaar EP, Gaspar AH, Humayun M, Gornicki P, Jelenska J, Joachmiak A, Missiakas DM, Schneewind O. 2003. Passage of heme-iron across the envelope of *Staphylococcus aureus*. *Science* 299:906–909. <https://doi.org/10.1126/science.1081147>.
 27. Schlag S, Fuchs S, Nerz C, Gaupp R, Engelmann S, Liebeke M, Lalk M, Hecker M, Götz F. 2008. Characterization of the oxygen-responsive NreABC regulon of *Staphylococcus aureus*. *J Bacteriol* 190:7847–7858. <https://doi.org/10.1128/JB.00905-08>.
 28. Overbeek R, Fonstein M, D'Souza M, Pusch GD, Maltsev N. 1999. The use of gene clusters to infer functional coupling. *Proc Natl Acad Sci U S A* 96:2896–2901. <https://doi.org/10.1073/pnas.96.6.2896>.
 29. Chang W, Small DA, Toghiani F, Bentley WE. 2006. Global transcriptome analysis of *Staphylococcus aureus* response to hydrogen peroxide. *J Bacteriol* 188:1648–1659. <https://doi.org/10.1128/JB.188.4.1648-1659.2006>.
 30. Horsburgh MJ, Clements MO, Crossley H, Ingham E, Foster SJ. 2001. PerR controls oxidative stress resistance and iron storage proteins and is required for virulence in *Staphylococcus aureus*. *Infect Immun* 69:3744–3754. <https://doi.org/10.1128/IAI.69.6.3744-3754.2001>.
 31. Kinkel TL, Roux CM, Dunman PM, Fang FC. 2013. The *Staphylococcus aureus* SrrAB two-component system promotes resistance to nitrosative stress and hypoxia. *mBio* 4:e00696-13. <https://doi.org/10.1128/mBio.00696-13>.
 32. Wang L, Elliott M, Elliott T. 1999. Conditional stability of the HemA protein (glutamyl-tRNA reductase) regulates heme biosynthesis in *Salmonella typhimurium*. *J Bacteriol* 181:1211–1219.
 33. Jones AM, Elliott T. 2010. A purified mutant HemA protein from *Salmonella enterica* serovar Typhimurium lacks bound heme and is defective for heme-mediated regulation *in vivo*. *FEMS Microbiol Lett* 307:41–47. <https://doi.org/10.1111/j.1574-6968.2010.01967.x>.
 34. Wang L, Wilson S, Elliott T. 1999. A mutant HemA protein with positive charge close to the N terminus is stabilized against heme-regulated proteolysis in *Salmonella typhimurium*. *J Bacteriol* 181:6033–6041.
 35. Laakso HA, Marolda CL, Pinter TB, Stillman MJ, Heinrichs DE. 2016. A heme-responsive regulator controls synthesis of staphyloferrin B in *Staphylococcus aureus*. *J Biol Chem* 291:29–40. <https://doi.org/10.1074/jbc.M115.696625>.
 36. Dutter BF, Mike LA, Reid PR, Chong KM, Ramos-Hunter SJ, Skaar EP, Sulikowski GA. 2016. Decoupling activation of heme biosynthesis from anaerobic toxicity in a molecule active in *Staphylococcus aureus*. *ACS Chem Biol* 11:1354–1361.
 37. Mike LA, Dutter BF, Stauff DL, Moore JL, Vitko NP, Aranmolate O, Kehl-Fie TE, Sullivan S, Reid PR, DuBois JL, Richardson AR, Caprioli RM, Sulikowski GA, Skaar EP. 2013. Activation of heme biosynthesis by a small molecule that is toxic to fermenting *Staphylococcus aureus*. *Proc Natl Acad Sci U S A* 110:8206–8211. <https://doi.org/10.1073/pnas.1303674110>.
 38. Surdel MC, Horvath DJ, Jr, Lojek LJ, Fullen AR, Simpson J, Dutter BF, Salleng KJ, Ford JB, Jenkins JL, Nagarajan R, Teixeira PL, Albertolle M, Georgiev IS, Jansen ED, Sulikowski GA, Lacy DB, Dailey HA, Skaar EP. 2017. Antibacterial photosensitization through activation of coproporphyrinogen oxidase. *Proc Natl Acad Sci U S A* 114:E6652–E6659. <https://doi.org/10.1073/pnas.1700469114> pii: 201700469.
 39. Girvan HM, Munro AW. 2013. Heme sensor proteins. *J Biol Chem* 288:13194–13203. <https://doi.org/10.1074/jbc.R112.422642>.
 40. Zhao A, Fang Y, Chen X, Zhao S, Dong W, Lin Y, Gong W, Liu L. 2014. Crystal structure of *Arabidopsis* glutamyl-tRNA reductase in complex with its stimulator protein. *Proc Natl Acad Sci U S A* 111:6630–6635. <https://doi.org/10.1073/pnas.1400166111>.
 41. Apitz J, Nishimura K, Schmied J, Wolf A, Hedtke B, van Wijk KJ, Grimm B. 2016. Posttranslational control of ALA synthesis includes GluTR degradation by Clp protease and stabilization by GluTR-binding protein. *Plant Physiol* 170:2040–2051. <https://doi.org/10.1104/pp.15.01945>.
 42. Skaar EP, Humayun M, Bae T, DeBord KL, Schneewind O. 2004. Iron-source preference of *Staphylococcus aureus* infections. *Science* 305:1626–1628. <https://doi.org/10.1126/science.1099930>.
 43. Jensen J. 1962. The effect of heme on tetrapyrrole synthesis in a heme requiring *Staphylococcus aureus*. *Biochem Biophys Res Commun* 8:271–277. [https://doi.org/10.1016/0006-291X\(62\)90276-0](https://doi.org/10.1016/0006-291X(62)90276-0).
 44. Bae T, Schneewind O. 2006. Allelic replacement in *Staphylococcus aureus* with inducible counter-selection. *Plasmid* 55:58–63. <https://doi.org/10.1016/j.plasmid.2005.05.005>.
 45. Choby JE, Mike LA, Mashruwala AA, Dutter BF, Dunman PM, Sulikowski GA, Boyd JM, Skaar EP. 2016. A small-molecule inhibitor of iron-sulfur cluster assembly uncovers a link between virulence regulation and metabolism in *Staphylococcus aureus*. *Cell Chem Biol* 23:1351–1361. <https://doi.org/10.1016/j.chembiol.2016.09.012>.
 46. Fey PD, Endres JL, Yajjala VK, Widhelm TJ, Boissy RJ, Bose JL, Bayles KW. 2013. A genetic resource for rapid and comprehensive phenotype screening of nonessential *Staphylococcus aureus* genes. *mBio* 4:e00537-12. <https://doi.org/10.1128/mBio.00537-12>.
 47. Kardon JR, Yien YY, Huston NC, Branco DS, Hildick-Smith GJ, Rhee KY, Paw BH, Baker TA. 2015. Mitochondrial ClpX activates a key enzyme for heme biosynthesis and erythropoiesis. *Cell* 161:858–867. <https://doi.org/10.1016/j.cell.2015.04.017>.
 48. Vitko NP, Richardson AR. 2013. Laboratory maintenance of methicillin-resistant *Staphylococcus aureus* (MRSA). *Curr Protoc Microbiol* Chapter 9:Unit 9C.2. <https://doi.org/10.1002/9780471729259.mc09c02s28>.
 49. Blaxter M, Mann J, Chapman T, Thomas F, Whitton C, Floyd R, Abebe E. 2005. Defining operational taxonomic units using DNA barcode data. *Philos Trans R Soc Lond B Biol Sci* 360:1935–1943. <https://doi.org/10.1098/rstb.2005.1725>.
 50. Jones M, Ghoorah A, Blaxter M. 2011. jMOTU and Taxonomator: turning DNA barcode sequences into annotated operational taxonomic units. *PLoS One* 6:e19259. <https://doi.org/10.1371/journal.pone.0019259>.
 51. Overbeek R, Begley T, Butler RM, Choudhuri JV, Chuang HY, Cohoon M,

- de Crécy-Lagard V, Diaz N, Disz T, Edwards R, Fonstein M, Frank ED, Gerdes S, Glass EM, Goesmann A, Hanson A, Iwata-Reuyl D, Jensen R, Jamshidi N, Krause L, Kubal M, Larsen N, Linke B, McHardy AC, Meyer F, Neuweger H, Olsen G, Olson R, Osterman A, Portnoy V, Pusch GD, Rodionov DA, Rückert C, Steiner J, Stevens R, Thiele I, Vassieva O, Ye Y, Zagnitko O, Vonstein V. 2005. The subsystems approach to genome annotation and its use in the project to annotate 1000 genomes. *Nucleic Acids Res* 33:5691–5702. <https://doi.org/10.1093/nar/gki866>.
52. Overbeek R, Olson R, Pusch GD, Olsen GJ, Davis JJ, Disz T, Edwards RA, Gerdes S, Parrello B, Shukla M, Vonstein V, Wattam AR, Xia F, Stevens R. 2014. The SEED and the Rapid Annotation of microbial genomes using Subsystems Technology (RAST). *Nucleic Acids Res* 42:D206–D214. <https://doi.org/10.1093/nar/gkt1226>.
53. Ciccarelli FD, Doerks T, von Mering C, Creevey CJ, Snel B, Bork P. 2006. Toward automatic reconstruction of a highly resolved tree of life. *Science* 311:1283–1287. <https://doi.org/10.1126/science.1123061>.
54. Thompson JD, Higgins DG, Gibson TJ. 1994. CLUSTAL W: improving the sensitivity of progressive multiple sequence alignment through sequence weighting, position-specific gap penalties and weight matrix choice. *Nucleic Acids Res* 22:4673–4680. <https://doi.org/10.1093/nar/22.22.4673>.
55. Jones DT. 2007. Improving the accuracy of transmembrane protein topology prediction using evolutionary information. *Bioinformatics* 23: 538–544. <https://doi.org/10.1093/bioinformatics/btl677>.
56. Krogh A, Larsson B, von Heijne G, Sonnhammer EL. 2001. Predicting transmembrane protein topology with a hidden Markov model: application to complete genomes. *J Mol Biol* 305:567–580. <https://doi.org/10.1006/jmbi.2000.4315>.
57. Duthie ES, Lorenz LL. 1952. Staphylococcal coagulase: mode of action and antigenicity. *J Gen Microbiol* 6:95–107. <https://doi.org/10.1099/00221287-6-1-2-95>.
58. Mayfield JA, Hammer ND, Kurker RC, Chen TK, Ojha S, Skaar EP, DuBois JL. 2013. The chlorite dismutase (HemQ) from *Staphylococcus aureus* has a redox-sensitive heme and is associated with the small colony variant phenotype. *J Biol Chem* 288:23488–23504. <https://doi.org/10.1074/jbc.M112.442335>.
59. Wakeman CA, Hammer ND, Stauff DL, Attia AS, Anzaldi LL, Dikalov SI, Calcutt MW, Skaar EP. 2012. Menaquinone biosynthesis potentiates haem toxicity in *Staphylococcus aureus*. *Mol Microbiol* 86:1376–1392. <https://doi.org/10.1111/mmi.12063>.
60. Stauff DL, Skaar EP. 2009. *Bacillus anthracis* HssRS signalling to HrtAB regulates haem resistance during infection. *Mol Microbiol* 72:763–778. <https://doi.org/10.1111/j.1365-2958.2009.06684.x>.
61. Attia AS, Benson MA, Stauff DL, Torres VJ, Skaar EP. 2010. Membrane damage elicits an immunomodulatory program in *Staphylococcus aureus*. *PLoS Pathog* 6:e1000802. <https://doi.org/10.1371/journal.ppat.1000802>.
62. Kreiswirth BN, Löfdahl S, Betley MJ, O'Reilly M, Schlievert PM, Bergdoll MS, Novick RP. 1983. The toxic shock syndrome exotoxin structural gene is not detectably transmitted by a prophage. *Nature* 305:709–712. <https://doi.org/10.1038/305709a0>.